ADAPTIVE MULTIGRID MODELLING OF DENSITY DEPENDENT GROUNDWATER FLOW

John M. VAN ESCH

GeoDelft, Stieltjesweg 2
NL-2600 AB Delft, THE NETHERLANDS
J.M.vanEsch@geodelft.nl

ABSTRACT

This paper presents a new modelling technique that can be used for solving groundwater flow problems that are dominated by density effects due to solute transport or thermal flow. The technique combines the finite element method for discretizing the coupled flow and transport equation and a multigrid approach for solving the generated matrix-vector equation using a hierarchy of finite element meshes. Instead of using static grids in the refinement sequence only grid cells for which the element Peclet number exceeds a threshold value or the mass fraction gradient is high, are replaced by finer elements. This approach is capable of locating a sharp front and refining the mesh in this zone only, leaving the mesh course in the rest of the domain. The modelling technique is demonstrated for two verification tests: Henry's problem and Elder's problem. These verification tests show that the time dependent behaviour of the brackish zone between salt and fresh groundwater can be predicted efficiently for stable situations with fine grid accuracy. However result are slightly unpredictable for unstable situation. For these flow conditions coarse grid solutions mix with fine grid results. Future research will focus on this phenomenon and will be related to optimization of the multi grid cycle. The algorithm leads to an efficient use of computer resources, especially for three-dimensional situations. The model can already be applied to practical problems, for instance to optimise the operation of deep well infiltration systems as described by Van Esch and Stakelbeek [SWIM 96].

MATHEMATICAL MODEL

Bear and Verruijt [1] present the derivation of the governing equation that describes (un)saturated groundwater flow. The flow equation combines a mass balance equation and Darcy's law and is known as the Richards equation

$$\frac{\partial}{\partial t}(nS\rho) = \frac{\partial}{\partial x_i}\left[\frac{\rho k K_{ij}}{\mu}\left(\frac{\partial p}{\partial x_j} - \rho g_j\right)\right] \qquad (1)$$

In this equation pressure p [Pa] is the primary unknown, the independent variables are x [m] specifying the position in space along the Cartesian coordinate axis and time t [s]. The fluid density ρ [kgm^{-3}] and its dynamic viscosity μ [kgm^{-1}s^{-1}] may depend on pressure and vary with the amount of solute dissolved in the liquid phase. Porosity n [-] and the saturated hydraulic conductivity tensor K [m^2] are assumed to be related to the soil only and vary in space only. The water content is described as the product of porosity and saturation S [-] that is related to fluid pressure and soil type. The relative permeability k [-] is related to saturation and soil type. Acceleration due to gravity is expressed by the gravity vector g [ms^{-2}] pointing downward in the third coordinate direction. Source terms are included as boundary conditions, leading to a more general approach. The flow equation can be interpreted as the transport equation for the fluid containing all solutes. The transport equation for a single component reads

$$\frac{\partial}{\partial t}(nS\omega\rho) = -\frac{\partial}{\partial x_i}(\omega\rho q_i) + \frac{\partial}{\partial x_i}\left(\rho D_{ij}\frac{\partial \omega}{\partial x_j}\right) \qquad (2)$$

The primary unknown in this equation is the solute mass fraction ω [-]. The first term on the right hand side includes the convective flux, the second term includes the dispersive flux. As the model must be capable to handle high-density differences the Oberbeck-Boussinesq condition, which states that changes in density can be neglected except for the buoyancy term ρg has not been applied. Also a linear combination of the transport equation and a multiple ω of the flow equation does not replace the original transport equation, although the differential rule on the convective term has to be applied later on in the numerical derivation.

For so-called uncoupled situations the velocity field can be obtained from the flow equation. The volumetric Darcy flux q [ms^{-1}] reads

$$q_i = -\frac{kK_{ij}}{\mu}\left(\frac{\partial p}{\partial x_j} - \rho g_j\right) \tag{3}$$

The real velocity vector is calculated from the Darcy velocity as $v = q/nS$. The vector field ties the flow equation to the transport equation. The hydrodynamic dispersion tensor D [m^{2}s^{-1}] is generally related to the molecular diffusion d_m [m^{2}s^{-1}] and the Darcy velocity field as

$$D_{ij} = nSd_m\delta_{ij} + (\alpha_l - \alpha_t)\frac{q_i q_j}{q} + \alpha_t q\delta_{ij} \tag{4}$$

Longitudinal dispersivity α_l [m] and transversal dispersivity α_t [m] introduce mechanical mixing. A non-linear extension of the Fickian dispersion equation given by Hassanizadeh that should be used when high concentration gradients are present has not been implemented. The extension has the same form as the Forchheimer equation for high velocity, the high concentration coefficient resembles the Forchheimer coefficient. A lack of knowledge concerning the high concentration coefficient restricts its applicability to real situations.

Van Genuchten [6] presents a popular material model for saturation and relative permeability. For saturation his expression reads

$$S = S^r + (S^s - S^r)\cdot\left[1 + (g_a|p|)^{g_n}\right]^{-g_m} \tag{5}$$

According to this description saturation varies between the residual saturation S^r [-] and maximum saturation S^s [-]. The relation holds for negative pressures and is only C_0 continuous for $p=0$. The expression for relative permeability is given by

$$k = (S^e)^{g_l}\left[1 - \left(1 - (S^e)^{1/g_m}\right)^{g_m}\right]^2 \tag{6}$$

Here relative permeability is related to saturation using the effective saturation S^e [-] written as $S^e = (S-S^r)/(S^s-S^r)$. The Van Genuchten material model contains three parameters: g_a [Pa^{-1}], g_l [-] and g_n [-] that are obtained from laboratory experiments and a fitting procedure. The missing parameter $g_m = 1-1/g_n$ will always be positive as $g_n > 1$.

The fluid density is usually given as a functional relation with pressure and solute mass fraction as

$$\rho = \rho^0 \exp\left[\beta^p\left(p - p^0\right) + \beta^\omega(\omega)\right] \tag{7}$$

The reference density $\rho^0 = 9.981\cdot10^2$ kgm^{-3} of fresh water is determined at a prescribed pressure $p^0 = 10^5$ Pa and solute mass fraction $\omega = 0$. For a fluid with dissolved salt the coefficients values $\beta^p = 4.5\cdot10^{-10}$ Pa^{-1} and $\beta^\omega = 0.7$ are found at a temperature of 20°C. The viscosity of the fluid mainly depends on solute mass fraction

$$\mu = \mu^0 \left(a_0 + a_1 \omega + a_2 \omega^2 \right) \tag{8}$$

The reference viscosity μ^0 [kgm^{-1}s^{-1}] is determined for the fluid without any solute. The polynomial coefficients for dissolved salt are given by 1.0, 1.85 and –4.0.

Since saturation, relative permeability fluid density and viscosity are all related to pressure and solute mass fraction, the initial pressure field can be found from one of them and the inverse relation. The initial conditions may also be given as a prescribed pressure field

$$p(x,t^0) = \overline{p}^0 \quad in \quad \Omega \tag{9}$$

and mass fraction field

$$\omega(x,t^0) = \overline{\omega}^0 \quad in \quad \Omega \tag{10}$$

The two fields do not have to match each other and alternatively, an equilibrium condition can be calculated from a set of boundary conditions. With Ω the calculation domain, Γ its boundary, and an overline denoting a given value. Three types of boundary conditions are presented here concerning the flow equation. Dirichlet boundary conditions prescribe a given pressure as

$$p = \overline{p}(x,t) \quad on \quad \Gamma_1^p \tag{11}$$

Neumann boundary conditions have no physical meaning for this problem, Cauchy conditions prescribe an out-flowing mass flux $\rho\bar{q}$

$$-\frac{\rho k K_{ij}}{\mu}\left(\frac{\partial p}{\partial x_j} + \rho g_j \right) n_i = \rho \overline{q}(x,t) \quad on \quad \Gamma_2^p \tag{12}$$

Only for an in-flowing fluid the right hand side mass density is known in advance, closed boundaries are formulated with a zero right hand side. Variable boundary conditions describe seepage where outflow takes place at atmospheric pressure, or precipitation in which case ponding may occur. Both conditions can be written as

$$\begin{cases} p = \overline{p}(x,t), & -\dfrac{\rho k K_{ij}}{\mu}\left(\dfrac{\partial p}{\partial x_j} + \rho g_j \right) n_i > \rho \overline{q}(x,t) \\ -\dfrac{\rho k K_{ij}}{\mu}\left(\dfrac{\partial p}{\partial x_j} + \rho g_j \right) n_i = \rho \overline{q}(x,t), & p < \overline{p}(x,t) \end{cases} \quad on \quad \Gamma_3^p \tag{13}$$

Conform this notation, the volumetric precipitation in-flux has a negative sign ($\bar{q} < 0$). The pressure $\bar{p}$ at which ponding takes place will be zero for the seepage face without precipitation ($\bar{q} = 0$). Time varying boundary conditions due to a fluctuating water level may switch from Γ_1 to Γ_3 and vice versa. In addition to the transport equation four types of boundary conditions will be presented here. Dirichlet boundary conditions prescribe a given mass fraction as

$$\omega = \overline{\omega}(x,t) \quad on \quad \Gamma_1^\omega \tag{14}$$

Neumann boundary conditions specify a diffusive out-flux, these conditions will generally be applied for the definition of a weak out-flowing condition that prevents wiggles. In that case the right hand side of the next formulation is zero

$$-\rho D_{ij}\frac{\partial \omega}{\partial t}n_i = \omega\rho\bar{q}(x,t) \quad on \quad \Gamma_2^{\omega} \tag{15}$$

Cauchy conditions could also prescribe an out-flowing mass flux $\omega\rho\bar{q}$

$$\left(\omega\rho q_i - \rho D_{ij}\frac{\partial \omega}{\partial x_j}\right)n_i = \omega\rho\bar{q}(x,t) \quad on \quad \Gamma_3^{\omega} \tag{16}$$

Only for an in-flowing fluid the right hand side mass density is known in advance. Closed boundaries are formulated with a zero right hand side. Variable boundary conditions are used for situations where no a-priori information is available about in-flowing or out-flowing takes place

$$\begin{cases} -\rho D_{ij}\dfrac{\partial \omega}{\partial t}n_i = \omega\rho q_i n_i(x,t), & -\dfrac{\rho k K_{ij}}{\mu}\left(\dfrac{\partial p}{\partial x_j}+\rho g_j\right)n_i > 0 \\ \left(\omega\rho q_i - \rho D_{ij}\dfrac{\partial \omega}{\partial x_j}\right)n_i = \overline{\omega\rho} q_i n_i(x,t), & -\dfrac{\rho k K_{ij}}{\mu}\left(\dfrac{\partial p}{\partial x_j}+\rho g_j\right)n_i \le 0 \end{cases} \quad on \quad \Gamma_4^{\omega} \tag{17}$$

Physically meaningful boundary conditions are constructed as a combination of flow and transport conditions. Inflowing conditions may follow from a combination of negative $\rho\bar{q}$ on Γ_2^p and negative $\omega\rho\bar{q}$ on Γ_3^{ω} or p on Γ_1^p and $\omega\rho$ on Γ_4^{ω}.

NUMERICAL MODEL

The finite element method is well explained by Hughes [3] and Huyakorn ea. [4], and will not be presented in detail here. In the following paragraph only bi-linear quadrilateral elements and tri-linear hexahedral elements are used to subdivide the modelling domain. However the implemented model is more general. In this paragraph the numerical model will be presented for the flow equation and transport equation separately as a sequential solution strategy will be used. The sets of discrete equations are based on standard conformal finite element discretization and fully implicit finite difference time stepping is applied. Following this approach the flow equation is written as

$$M_{ab}^{k+1}\frac{p_b^{k+1}-p_b^k}{\Delta t} + S_{ab}^{k+1}p_b^{k+1} = F_a^{k+1} \tag{18}$$

In the set of equations superscript k denotes the current time step. A mass conservative formulation is obtained by the use of tangential derivatives

$$\left.\frac{dn\rho S}{dp}\right|^{\omega^{k+1}} = \frac{(n\rho S)^{p^{k+1},\omega^{k+1}} - (n\rho S)^{p^k,\omega^{k+11}}}{p^{k+1}-p^k} \tag{19}$$

On convergence the original time derivative term will be approximated as $d(n\rho S)/dt \approx (2nS\rho^{pk+1,\omega k+1} - nS\rho^{pk+1,\omega k} - nS\rho^{pk,\omega k+1})/\Delta t$. The transport equation contains the same approximation $d(n\omega\rho S) \approx (2nS\omega\rho^{pk+1,\omega k+1} - nS\omega\rho^{pk+1,\omega k} - nS\omega\rho^{pk,\omega k+1})/\Delta t$. Partly unsaturated zones prevent the use of as $d(n\rho S)/dt \approx (nS\rho^{pk+1,\omega k+1} - nS\rho^{pk,\omega k})/\Delta t$ in the right hand side.

The components of the mass matrix M_{ab} are given as

$$M_{ab} = \int_{\Omega} N_a N_b \left.\frac{dn\rho S}{dp}\right|^{\omega^{k+1}} d\Omega \tag{20}$$

According to the Galerkin condition the weighting function N_a is taken conform the interpolation function N_b. The value of the capacity matrix for water content change is evaluated numerically. Row sum lumping of the matrix improves the stability of the algorithm. The stiffness matrix S_{ab} reads

$$S_{ab} = \int_{\Omega} \frac{\rho k K_{ij}}{\mu} \frac{\partial N_a}{\partial x_i} \frac{\partial N_b}{\partial x_j} d\Omega \tag{21}$$

This contribution is found using Green's theorem for order reduction. Order reduction also contributes to the force vector F_a components

$$F_a = \int_{\Omega} \rho g_j \frac{\rho k K_{ij}}{\mu} \frac{\partial N_a}{\partial x_i} d\Omega - \int_{\Omega} N_a N_b \frac{dn\rho S}{d\omega}\Big|^{p^{k+1}} \left(\omega_b^1 - \omega_b^0\right) d\Omega - \int_{\Gamma_{2,3}} N_a \rho \bar{q} d\Gamma \tag{22}$$

Integration is performed numerically by Gaussian quadrate. The non-linear equations are linearized using a Picard method

$$\left(M_{ab}^{k+1,r} + \Delta t\, S_{ab}^{k+1,r}\right) p_b^{k+1,r+1} = M_{ab}^{k+1,r} p_b^k + \Delta t\, F_a^{k+1,r} \tag{23}$$

Superscript r denotes the current iterate. This process is repeated until a convergence criterion is met, stated as $|p^{r+1}-p^r| - \varepsilon_1 |p^1 - p^0| < \varepsilon_0$, where the vector norm has been used.

The transport equation is treated in the same way

$$M_{ab}^{k+1} \frac{\omega_b^{k+1} - \omega_b^k}{\Delta t} + S_{ab}^{k+1} \varpi_b^{k+1} = F_a^{k+1} \tag{24}$$

The components of the mass matrix M_{ab} are given by

$$M_{ab} = \int_{\Omega} N_a N_b \frac{dn\rho S}{dp}\Big|^{p^{k+1}} d\Omega \tag{25}$$

The stiffness matrix S_{ab} reads

$$S_{ab} = -\int_{\Omega} \rho q_i \frac{\partial N_a}{\partial x_i} N_b d\Omega + \int_{\Omega} \alpha \rho q_l \frac{\partial N_a}{\partial x_l} \rho q_i \frac{\partial N_b}{\partial x_i} d\Omega + \int_{\Omega} \frac{\partial N_a}{\partial x_i} \frac{\partial N_b}{\partial x_j} \rho D_{ij} d\Omega \tag{26}$$

Streamline upwinding has only been applied to the convective term. A consistent approach would be to also apply it to the time derivative terms but then one should use it in the flow equation as well. Green's theorem leading to for order reduction was applied on the convective and the dispersive term Partial differentiation was carried out first on the original convective term making the equation suitable for SUPG. The force vector reads

$$F_a = -\int_{\Omega} N_a N_b \frac{dn\rho S}{dp}\Big|^{\omega^{k+1}} \left(p_b^{k+1} - p_b^k\right) d\Omega - \int_{\Gamma_{2,3}} N_a N_b \left(\omega \rho \bar{q}\right)_b d\Gamma - \int_{\Gamma_{2,3}} N_a N_b \left(\overline{\omega \rho q}\right)_b d\Gamma \tag{27}$$

The non-linear equations are linearized using again a Picard method

$$\left(M_{ab}^{k+1,r} + \Delta t\, S_{ab}^{k+1,r}\right)\omega_b^{k+1,r+1} = M_{ab}^{k+1,r}\,\omega_b^{k} + \Delta t\, F_a^{k+1,r} \tag{28}$$

The process is repeated until a convergence, stated as $|\omega^{r+1}-\omega^{r}|-\varepsilon_1|\omega^{1}-\omega^{0}|<\varepsilon_0$, where the vector norm has been used.

MULTI GRID SOLVER

Multi grid is well explained by Hackbusch [2]. The method uses a grid hierarchy and is designed to solve a set of equations in *O(n)* computational operations. For this problem, the Full Approximation Storage algorithm (FAS) is applied to resolve the non-linear set of equations generated per time step. By this approach Picard iteration is carried out on each level

$$A_{ab}^{p}\left(p^{r},\omega^{r}\right)p_b^{r+1} = B_a^{p,r}\left(p^{r},\omega^{r}\right),\quad A_{ab}^{\omega}\left(p^{r+1},\omega^{r}\right)\omega_b^{r+1} = B_a^{\omega,r}\left(p^{r+1},\omega^{r}\right) \tag{29}$$

Numerical experiments however indicate that a new update for the pressure can be used in the construction of the coarse grid operator but a restriction of the original values for the mass fractions should be used leading to just linear multi grid for the transport equation.

At first the solution is approximated on the finest grid and the high frequency errors are smoothed out for instance by Gauss-Seidel relaxation. Then a restriction operator transfers the approximated solution and a correction to residual vector to the next courser mesh. On this mesh again a number of relaxation sweeps take place until convergence slows down. This process is repeated until the lowest level is reached. On this level the solution can be calculated exactly in only a fraction of work that would be needed for the finest mesh. Now the prolongation operator transfers the low level results back to the next finer grid where post-smoothing takes place. During this upward stroke process only elements that meet a certain refinement criterion are actually refined. By adaptive gridding the highest level mesh contains only a subset of nodes initial defined on the fixed mesh making the problem easier to solve. However Figure 1 clearly shows that the transfer of nodal information can become rather complex. Elements belonging to a much lower level, may have to be refined as a consequence of refinement of neighbouring elements. This process is called regularization. Also information not available in the downward stroke may be needed in the upward stroke.

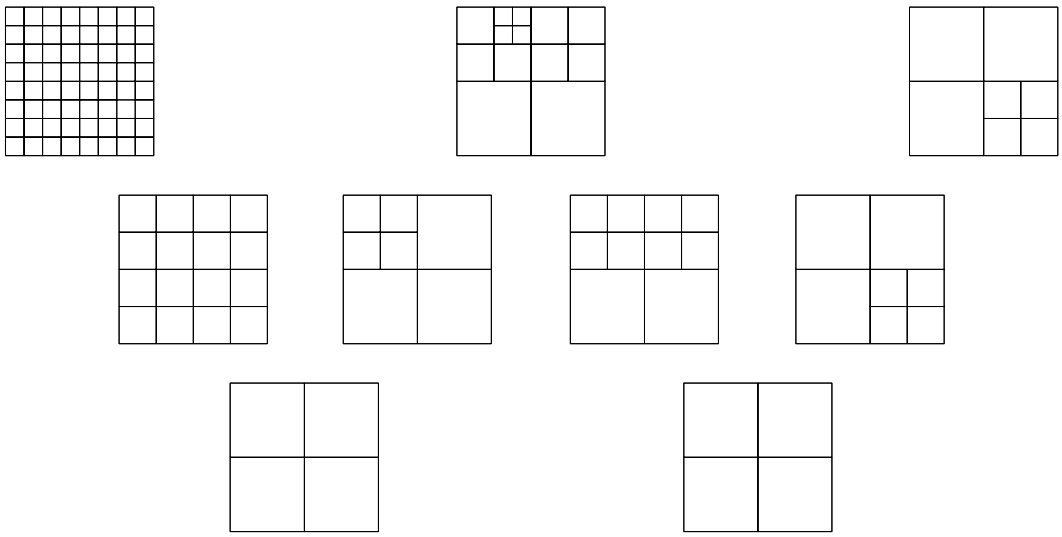

Figure 1 *Adaptive multi grid cycle*

As a criterion for refinement, the pressure gradient can be calculated. For the flow equation a better indication is found by reformulating the right hand side of Equation (1) using partial differentiation. For the resulting convection-diffusion type of equation the element Peclet number can be formulated as $Pe_i = \Delta x_i / k_{ii} \cdot \delta k / \delta x_i$. Its value depends only on the element size Δx [m] and relative permeability. The Peclet number for the transport equation is written as $Pe_i = v_i \Delta x_i / D_{ii}$ where v_i denotes the real velocity and D_{ii} the diagonal component of the dispersion tensor for the characteristic element size Δx_i in that direction. Analogous to the flow equation a mass fraction gradient could capture sharp fronts and is implemented as a second criterion. Care has to be taken with respect to the Courant number for which the time step can be selected $Cr = v \Delta t / \Delta x$, this criterion has to be fulfilled on the smallest grid whereas the number grows on finer grids. During the process, hanging grid points are generated. Hanging grid points (slave points) are handled by linear interpolation and correcting the equations for non-hanging (master points) in which the hanging grid points contribute.

VERIFICATION

This paragraph shows two classical verification tests: Henry's problem and Elder's problem. Both are specified on a two-dimensional domain, Henry's problem is solved on a three dimensional domain also to demonstrate the models applicability to these problems. Henry originally poses a density driven flow problem on a two dimensional domain of length l of 2 m, height h of 1 m. On the left boundary inflow of fresh water takes place at a rate of $6.6 \cdot 10^{-5}$ ms^{-1}. The density of the fresh water ρ_f is 10^3 kgm^{-3} at a salt mass fraction $\omega = 0$. The right boundary represents the seawater side. The salt-water density ρ_s equals 1025 kgm^{-3} and pressure varies linearly with elevation height as $p = \rho_s g h$, where the gravity constant g is taken as 9.8 ms^{-1}. Now a maximum pressure of $1.0045 \cdot 10^5$ Pa at the bottom of the boundary is found. Top and bottom boundaries are closed to flow and transport. The fluid density varies linearly with salt mass fraction as $\rho = \rho_f + 700 \omega$. Using this relation the salt mass fraction of seawater is found to be $3.571 \cdot 10^{-2}$. Intrinsic permeability κ of the porous medium is taken to be $1.020408\ 10^{-9}$ m^2 and porosity n equals 0.35. Mixing only takes place by molecular diffusion d_m with a value of $1.88571 \cdot 10^{-5}$ m^{2}s^{-1}, the fluids viscosity μ is taken constant as 10^{-3} Pas. Initially no salt is present in the domain and the pressure field follows from the flow boundary conditions. This may seem to be somewhat artificial, but the same situation can be reached in an infinite small time step as the domain is completely saturated and the elastic storage terms are zero. Simulations where carried out on a mesh hierarchy of 10x5, 20x10 and 40x20 elements, generating 66, 231 and 861 nodes. On the coarsest mesh the element size is 0.2 m, time steps of 100 s are taken and a maximum velocity of $1.5 \cdot 10^{-3}$ m/s is found. The Peclet number Pe is 16 and 4 on the finest grid. The Courant number Cr varies from 0.75 on the coarse grid and 3 on the fine grid. Refinement of the mesh was carried on elements for which the gradient of the mass fraction exceeded a threshold value of 10^{-2}.

Figure 2 shows mass fraction contours for several time steps. At the lower right boundary inflow of denser seawater takes place, whereas at the upper right boundary outflow occurs. A transition zone forms the interface between salt and fresh water. The width of this zone depends on the diffusion coefficient and the rate of shear flow. The last figure shows the steady state solution. The results compare well with results presented in literature and those obtained by a fine grid model.

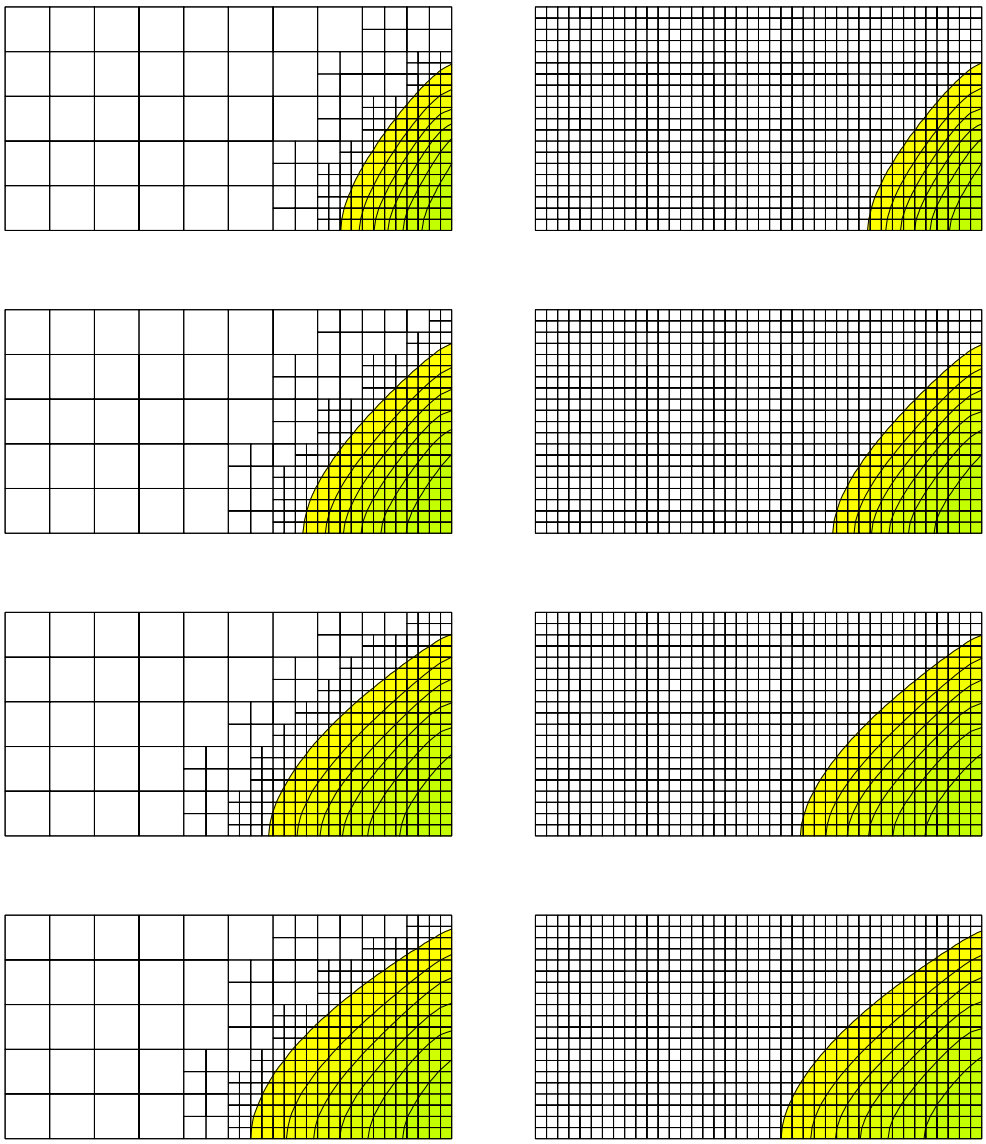

Figure 2 *Henry's problem results for t = 1e3, 2e3, 4e3 and 8e3 s, adaptive mesh and salinity contours for* ω *= 0.005, 0,010, 0.015, 0.020, 0.025, 0.030, 0.035 and 0.040.*

The model applicability to three-dimensional configurations is illustrated for the same problem. The mesh now contains 250 elements and 396 nodes on the first level and 4000 elements and 18.081 nodes on the third level. Figure 2 shows the adaptive mesh and salinity contours for 10^3 s. Both mesh and mass fraction results are identical to the results obtained for the two dimensional equivalent.

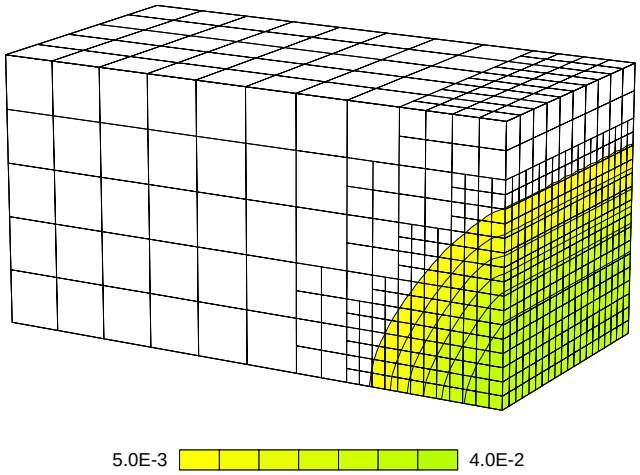

Figure 3 *Henry's problem results for t = 1e3s, adaptive mesh and salinity contours for ω = 0.005, 0,010, 0.015, 0.020, 0.025, 0.030, 0.035 and 0.040.*

Whereas Henry's problem forms a stable situation with fresh water on top of salt water, Elder's problem shows an example of an in-stable situation. Here a denser (mixable) fluid is placed on top of a less dense (mixable) fluid. The flow domain has a length *l* of 600 m and height *h* of 150 m. At the top of the domain 150 to 450 m the total fluid flux equals zero and the mass fraction ω is prescribed as 0.26. Except for the two top corner points the rest the boundary is closed for flow of the fluid, the mass fractions are set to zero however. To specify a well-posed problem in the top corner points the pressure is set to an arbitrary value 10^5 Pa. These points provide the only spots where outflow can take place, the mass fraction follows from the out-flowing fluid. The fresh water density ρ_f equals 10^3 kgm^{-3} and brine density ρ_f is $1.2 \cdot 10^3$ kgm^{-3} at salt mass fraction ω of 0.26. Between these values the fluid density varies linearly as $\rho = \rho_f + 769.2\omega$, fluid viscosity μ is set at a constant value of 10^{-3} Pas. The intrinsic permeability κ of the flow domain is 4.845 10^{-13} m^2 and porosity *n* is 0.1. The molecular diffusion coefficient for this case is $3.565 \cdot 10^{-6}$ m^{2}s^{-1}. The gravity field is given by the gravity constant 9.807 ms^{-2}. Calculations were carried out on a mesh hierarchy of three levels. Level 1 mesh contains 16x8 elements and 128 nodes, the third level mesh is constructed from 64x32 elements and 2048 nodes. The element size varies from 18.75 m down to 4.6875 m, the time step size was taken constant and set to 0.1 year. Calculations show a global maximum velocity of $3 \cdot 10^{-6}$ ms^{-1}, for this value the Peclet number equals 16 on level 3 and 4 on level 1, the Courant numbers were calculated as 0.25 and 2.

Initially the salt mass fractions are zero in the entire domain, leading to a hydrostatic pressure distribution. Figure 4 shows some transient results for the solute mass fraction on half the modelling domain. At first two eddies emerge on both sides of the dissolving salt boundary ends, initiating a downward flow. At about two years two smaller fingers start to grow in a rotational flow field where eight eddies are present. At later times the two small eddies become almost invisible and the small and large salt finger move towards each other. Finally two large eddies melt together and form one roll. The steady state solution thus shows two rolls for the complete modelling domain, in the centre of the domain the flow direction is pointing downward. In contrast to Elders findings only two fingers occur in half the modelling region (Elder reports five in the complete modelling domain).

Calculations on a single grid showed that for the given discretization lengths, results vary with grid discretization used. Results become almost grid independent if the mesh is refined one more time by a factor two. Further investigations showed that results are also depended on the numerical model that is used. The preferred way (in absence of partly saturated regions) for approximating the mass matrix as $d(nS\rho)/dt \approx [(nS\rho)k+1-(nS\rho)k] / \Delta t$ and $d(nS\omega\rho)/dt \approx [(nS\omega\rho)k+1-(nS\omega\rho)k] / \Delta t$ leads to basically the same patterns. Leijnse who uses this approximation, stated that mesh independent output could be found for grid with more than 4000 elements. This has still to be confirmed with presented algorithm in a one-mesh mode. A linear combination of the flow and transport equation to replace the transport equation gives different results that are equivalent to Sutra code results.

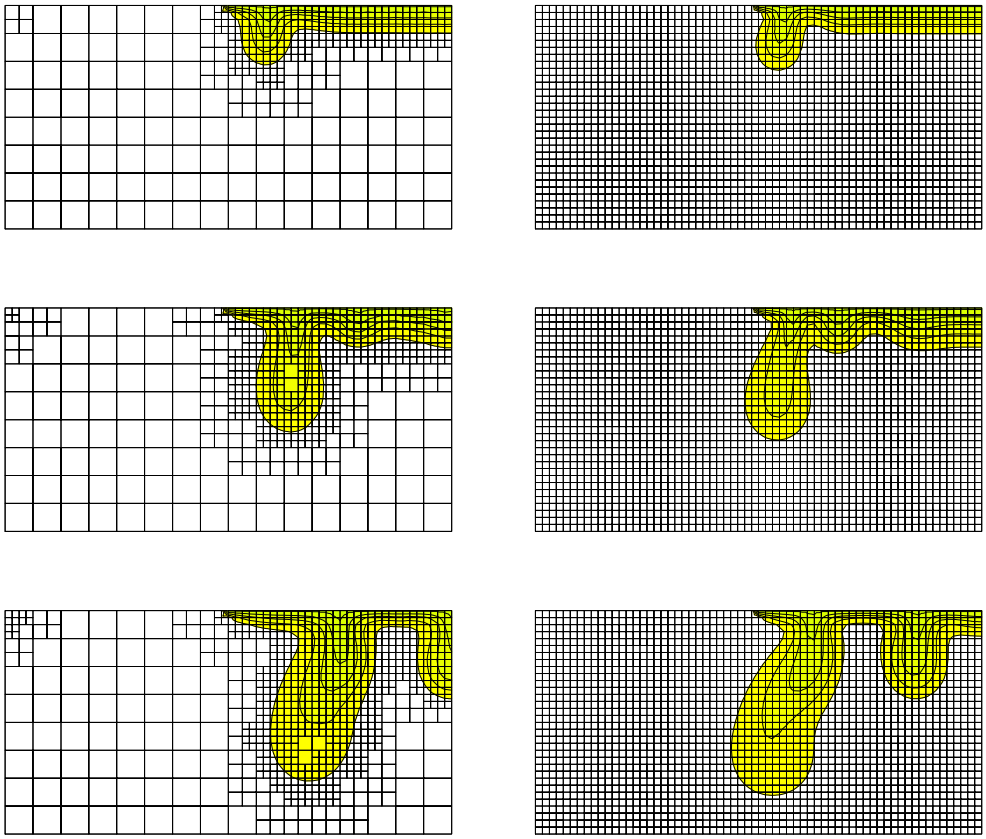

Figure 4 *Elder's problem results for t = 1, 2 and 3 year, adaptive mesh and salinity contours for* ω *= 0.05, 0.10, 0.15, 0.20, 0.25 and 0.30.*

If we now compare the results of the adaptive grid model using three mesh levels to the results using only one level we observe different flow patterns. In stable situations fine grid accuracy can be reached. For unstable cases coarse grid solutions mix with fine grid results. These conclusions can also be drawn for results of a non-adaptive setting of the multi grid solver. The problem may be of a more fundamental nature and depends on the ratio of density-induced convection on (numerical) diffusion.

The Rayleigh number of the system $Ra = (\kappa_{zz} g \Delta\rho L)/(\mu D)$ (or more general $Ra = (\kappa_{zz} g \Delta\rho L)/(\mu \alpha_l v)$ for dispersive transport) that presents a relation between convective flow driven by the buoyancy term and diffusive or dispersive transport. When the Rayleigh number increases the first critical value is crossed the conductive solution becomes unstable, there may be an exchange of stability from conduction to convection. In Elders problem this situation occurs. In bifurcation theory this is called a pitchfork bifurcation. If the Rayleigh number is even further increased, the steady convection solution become unstable. Then oscillatory convection may occur which is also known as Hopf bifurcation. For

these situations a steady state cannot be reached as the solution switches between two modes. For even higher Rayleigh numbers the transition to chaotic regimes is observed. Heat transfer through a system is often characterized by the Nusselt number $Nu = Q_{conv}/Q_{cond}$ which presents the division of convective energy flux and conductive energy flux, both integrated over the system boundaries. For a saline case the analogue is known as the Sherwood number. The Rayleigh number characterizes a system by its physical properties, the Nusselt number characterizes behaviour of the system. Both may be presented in a *Ra*-*Nu* diagram where the relation only holds for a certain branch (and cell pattern or mode). Future research focuses on these phenomena.

CONCLUSIONS

Adaptive multi-grid modelling provides an efficient algorithm to solve density dependent groundwater flow problems especially for three-dimensional situations. Adaptive refinement based on a mass fraction gradient threshold combined with an element Peclet number criterion is capable of capturing sharp fronts. The technique thus increases the accuracy of the solution but leaves the mesh unchanged in the rest of the modelling domain thereby ensuring computational efficiency. In stable situations fine grid accuracy can be reached. However result are slightly unpredictable in unstable situation. For these situations coarse grid solutions mix with fine grid results. Future research focuses on this phenomenon, which will be related to optimization of the multi grid cycle. A dynamic homogenization process is suggested for unsaturated flow problem. Numerical simulations have shown that the algorithm is suitable for solving heterogeneous flow applications resulting from geological modelling of the subsoil and is capable of locating high permeability streaks.

REFERENCES

Bear J. and Verruijt, A.: Modelling groundwater flow and pollution, Reidel, Dordrecht, 1987.

Hackbush, W.: Multi-grid methods and applications, Springer, Berlin, 1980.

Hughes, T.J.R., The finite element method, linear static and dynamic finite element analysis, Dover Publications, Mineola, New York, 2000.

Huyakorn, P.S. and Pinder, G.F., Computational methods in subsurface flow, Academic Press, San Diego, 1983

Van Esch, Adaptive modelling of unsaturated groundwater flow, Learned and applied, soil mechanics out of Delft, Balkema Publishers, Lisse, 2002.

Van Genuchten. M. Th.: A closed form equation for predicting the hydraulic function of unsaturated soils, Journal Soil Science Society of America, 44, 1980.